Research article

XiaoFei Zang, BingShuang Yao, Zhen Li, Yang Zhu, JingYa Xie, Lin Chen, Alexey. V. Balakin, Alexander. P. Shkurinov, YiMing Zhu* and SongLin Zhuang

Geometric phase for multidimensional manipulation of photonics spin Hall effect and helicity-dependent imaging

Abstract: The spin Hall effect of light, associated with spin-orbit interactions, describes a transport phenomenon with optical spin-dependent splitting, leading to a plethora of applications such as sensing, imaging, and spin-controlled nanophotonics. Although geometric meatsurfaces can mimic photonic spin Hall effect by spatially splitting left-hand circularly polarized and right-hand circularly polarized states of electromagnetic waves with anomalous refraction or reflection angles, the geometric phase generated by metasurfaces hinders metalenses to realize simultaneous focusing of different spin states, limiting further applications. Here, we propose and experimentally demonstrate an approach to realizing a spin Hall metalens that can focus terahertz waves with different spin states and flexibly manipulate spin-dependent focal points in multiple spatial dimensions based on a pure geometric phase. A dielectric metasurface consisting of micropillars with identical shape and different in-plane orientations is designed to realize the multidimensional manipulation of photonics spin Hall effect in terahertz region. Furthermore, helicity-dependent imaging is demonstrated by the terahertz spin Hall metalens. The uniqueness and robust approach for manipulating spin photons may have a significant impact on designing ultra-compact and multifunctional devices and spin photonics devices.

Keywords: geometry phase; helicity-dependent imaging; metalens; photonics spin Hall effect.

*Corresponding author: YiMing Zhu, Terahertz Technology Innovation Research Institute, Terahertz Spectrum and Imaging Technology Cooperative Innovation Center, Shanghai Key Lab of Modern Optical System, University of shanghai for Science and Technology, Shanghai, 200093, China; and Shanghai Institute of Intelligent Science and Technology, Tongji University, Shanghai, 200092, China, E-mail: ymzhu@usst.edu.cn. https://orcid.org/0000-0001-8557-895X
XiaoFei Zang and Lin Chen: Terahertz Technology Innovation Research Institute, Terahertz Spectrum and Imaging Technology Cooperative Innovation Center, Shanghai Key Lab of Modern Optical System, University of shanghai for Science and Technology, Shanghai, 200093, China; Shanghai Institute of Intelligent Science and Technology, Tongji University, Shanghai, 200092, China
BingShuang Yao, Zhen Li, Yang Zhu, JingYa Xie and SongLin Zhuang: Terahertz Technology Innovation Research Institute, Terahertz Spectrum and Imaging Technology Cooperative Innovation Center, Shanghai Key Lab of Modern Optical System, University of shanghai for Science and Technology, Shanghai, 200093, China
Alexey. V. Balakin and Alexander. P. Shkurinov: Department of Physics and International laser Center, Lomonosov Moscow State University, Leninskie Gory 1, Moscow, 19991, Russia; ILIT RAS – Branch of the FSRC "Crystallography and Photonics" RAS, Svyatoozerskaya 1, Shatura, Moscow, 140700, Russia

1 Introduction

Photonics spin Hall effect (PSHE), a counterpart of spin Hall effect (SHE) in electronic systems, is associated with spin-orbit interactions (SOI) [1–4], which are the coupling between the spin angular momentum (SAM) and orbital angular momentum (OAM) of light. The PSHE describes a transport phenomenon of optical spin-dependent splitting, which is typically related to two kinds of geometric phases: Rytov–Vladimirskii–Berry (RVB) phase [1–3] and Pancharatnam–Berry (PB) phase [4]. The RVB phase is concerned to the evolution of the propagation direction of light, and thus, a spin-dependent shift is occurred when a light beam propagates at an interface between different media [5]. The PB phase is related to a change in the polarization of light and it is produced in a certain inhomogeneous anisotropic media to generate PSHE [6]. Recently, a plethora of methods and technologies, *i. e.*, weak measurements, multireflections, and interferometry, have been proposed and demonstrated to elicit the weak PSHE [7–9], leading to various applications such as precision measurement [10] and differential computing [11–14].

Metasurfaces, metamaterials of reduced dimensionality, can flexibly tailor the amplitude, phase and polarization of electromagnetic waves [15, 16, 15, 16], leading to a plethora of applications such as metalens [17–23], cloaking [24], holograms [25–32], waveplates [33–36], orbital angular momentum manipulation [37–40] and nonlinear optics [41–45]. Since metasurfaces consisting of anisotropic nanopillars/micropillars with spatially variant orientations can generate geometric phase, they provide a platform for manipulating the phase of light at subwavelength resolution. Thus, metasurfaces enable the functionality for generating both weak and remarkable phase discontinuities, opening a new avenue for developing both weak and strong PSHE-based applications. Recently, Zhou et al., have realized optical edge detection based on the weak PSHE generated by metasurfaces [46]. Furthermore, the metasurfaces-based weak PSHE is extended to realize differential operation, resulting in new applications in biological imaging and computer vision [47–49]. Benefiting from unprecedented properties of metasurfaces, various types of spin photonics devices based on strong PSHE, *i. e.*, directional polarization coupler [50], polarization-controlled surface plasmon polaritons [51], and metaspiral plasmonic lens [52], have been developed. In addition, metasurfaces can generate giant PSHE [53–58] by designing a dramatic phase-gradient based on the PB phase (it is defined as the geometric phase). The phase-gradient enables spatially splitting of left-hand circularly polarized (LCP) and right-hand circularly polarized (RCP) electromagnetic waves with anomalous refraction or reflection angles. However, the splitted spin-dependent beams cannot be simultaneously focused based on the traditional (PB-phase-based) metalens, which inevitably degrades the perceptive devices for spin-dependent applications. Recently, a method combining both geometric and dynamic phase, is proposed to simultaneously manipulate the LCP and RCP light [59, 60]. Unlike the previous methods dependent on both dynamic phase and geometric phase, we propose an approach to design spin Hall metalens that can focus terahertz (THz) waves with different spin states and flexibly manipulate spin-dependent focal points in multiple spatial dimensions based on the pure geometric phase. A dielectric metasurfaces consisting of identical micropillars with spatially variant orientations is utilized to realize the manipulation of PSHE in both transverse and longitudinal directions. As a proof-of-concept, helicity-dependent imaging based on the spin Hall metalens is also demonstrated. The robust and flexible approach for designing spin Hall metalens may find practical applications in imaging, sensing and spin photonics devices.

2 Design and methods

Figure 1 shows a schematic of multidimensional manipulation of photonic spin Hall effect: For the incidence of LCP/RCP THz waves, one focal point is observed and located at an arbitrary position (see Figure 1(a) and (b)). Under the illumination of a linearly polarized THz beam, the spin-dependent splitting in arbitrary transverse and longitudinal directions is observed (see Figure 1(c)). It should be noted that the dielectric metasurface (see Figure 1) consisting of micropillars with identical shape and spatially variant orientations is applied to generate the pure geometric phase for manipulating different spin states of photons in multiple dimensions. Unlike the traditional metalens that can focus the LCP light and defocus the RCP light and vice versa, our designed metalens can focus both the LCP and RCP components into arbitrary spatial positions, leading to spin-dependent splitting (focal points) in multiple dimensions. Therefore, the key to realize such a metalens is that a single metasurface can simultaneously focus LCP and RCP electromagnetic waves into different positions. For a linearly-polarized light beam, it can be considered as the superposition of both LCP and RCP components with identical amplitude, and the corresponding Jones vector can be written as:

$$E_{x-pol} = \frac{\sqrt{2}}{2}\left(\begin{pmatrix} 1 \\ i \end{pmatrix} + \begin{pmatrix} 1 \\ -i \end{pmatrix} \right). \tag{1}$$

To focus the LCP component, the phase profile for the metalens can be expressed as:

$$\varphi_{LCP} = \frac{2\pi}{\lambda} \sqrt{(x - x_i)^2 + (y - y_i)^2 + f_i^2} - f_i, \tag{2}$$

in which λ is the working wavelength and f_i is the focal length. (x_i, y_i) are the arbitrary coordinates in the x-y plane.

To focus the RCP component, the required phase distribution is governed by:

$$\varphi_{RCP} = -\left(\frac{2\pi}{\lambda} \sqrt{(x - x_j)^2 + (y - y_j)^2 + f_j^2} - f_j \right), \tag{3}$$

where f_j is the focal length and (x_j, y_j) are the arbitrary coordinates in the x-y plane.

In order to realize a spin Hall metalens that can flexibly manipulate photonic spin-dependent splitting in multiple dimensions based on the pure geometric phase, the total phase profile should combine the two phase profiles together and it can be expressed as [43]:
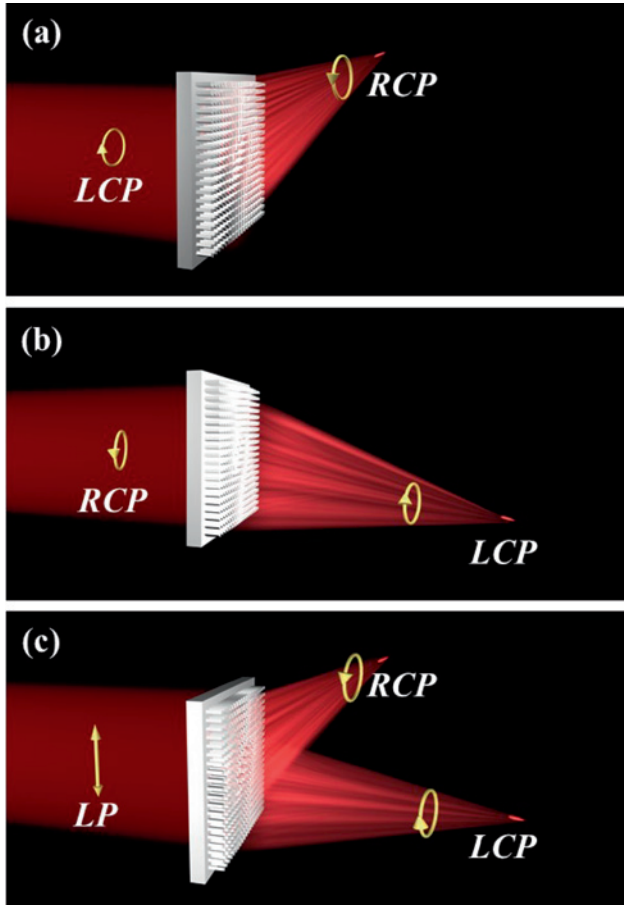
Figure 1: Schematic of the multidimensional manipulation of photonics SHE. (a)For the incidence of LCP THz waves, one RCP focal point is observed and located at an arbitrary position. (b) For the incidence of RCP THz waves, one LCP focal point is observed and located at an arbitrary position. (c) Under the illumination of linearly polarized THz waves, two separated spin-dependent (LCP and RCP) focal spots are manipulated and distributed in arbitrary positions. The arrays represent the polarization state of the THz waves.

$$\varphi_{total} = \arg\left[\exp\left(i\varphi_{LCP}\right) + \exp\left(i\varphi_{RCP}\right)\right]. \qquad (4)$$

The phase requirement in Eq. (4) contains two phase profiles: one is associated with focusing of LCP component, while the other is related to focusing of RCP component. It represents simultaneous as a convex lens and also as a concave lens under the illumination of LCP and RCP electromagnetic waves. The phase profile in Eq. (4) can be understood as follows: Under the illumination of linearly-polarized (LP) THz waves, two focal points with opposite circular-polarized states are observed after the spin Hall metalens. The corresponding field can be simply written as $\sim A e^{i\varphi_{LCP}}$ and $B e^{i\varphi_{RCP}}$. The total field of these two focal spots is $\sim A e^{i\varphi_{LCP}} + B e^{i\varphi_{RCP}}$. The phase requirement of these two focal spots is $\varphi_{total} = \arg\left[A \cdot \exp\left(i\varphi_{LCP}\right) + B \cdot \exp\left(i\varphi_{RCP}\right)\right]$

and we assume $A = B$ (they are the amplitude profiles of two focal spots). The detailed principle of spin Hall metalens is given in Supplementary Materials Section 1. The target phase in Eq. (4) consists of a convex lens and a concave lens (resulting in a diverging beam). Under the illumination of LCP THz wave, it interacts with two phase profiles: one phase profile (φ_{LCP}) enables the functionality for focusing the incident wave into a focal spot while the other phase profile (φ_{RCP}) defocus the incident wave. Therefore, only half of the transmitted waves are converted to the RCP focal spot. In contrast, for RCP incidence, half of the transmitted waves is converted to the LCP focal spot. Therefore, the maximal focusing efficiency of the designed metalens cannot exceed 50% in theory, which is an inherent limitation of the approach.

Figure 2(a) illustrates a schematic of the spin Hall metalens consisting of anisotropic silicon micropillars with predesigned in-plane orientations. Each pillar is considered as a quasi-perfect half-wave plate (see Ref [61]) with the optimized structural parameters as: $L = 85$ μm, $W = 40$ μm, $H = 500$ μm and $p = 110$ μm (period). The thickness of substrate is 500 μm and the working frequency of the metalens is 0.69 THz. Figure 2(b_1)~2(c_2) show the optical image of the designed metalenses with longitudinal spin-dependent splitting and multidimensional spin-dependent splitting, respectively. The near-field scanning terahertz microscopy (NSTM) [62–64] is utilized to detect the corresponding field distributions.

3 Results and discussion

As a guiding study, a metalens with longitudinal spin-splitting is initially demonstrated. Figure 3 shows the numerical simulation and experimental demonstration of such spin Hall metalens. The metalens consists of 100×100 micropillars. The corresponding structure parameters are as follows: $x_i = x_j = y_i = y_j = 0$, $f_i = 4$ mm and $f_j = 7$ mm. Figure 3(a_1) shows the calculated electric field ($|E|^2$) distribution of the designed metalens under the illumination of linearly-polarized (LP) THz waves with polarization along the x-axis (at 0.69 THz). Two separated focal points are observed along the longitudinal direction. The corresponding electric field distributions in the x-y plane are given in Figure 3(a_2) and 3(a_3), and there are two circular-shaped spots located at $z = 3.8$ mm and $z = 6.6$ mm, respectively (Here, the tail end of micropillars is defined as a reference plane to calculate the position of each focal spot). To further demonstrate the character of the spin-dependent splitting, the field distributions for LCP and RCP incidences are calculated. As shown by Figure 3(b_1) for the
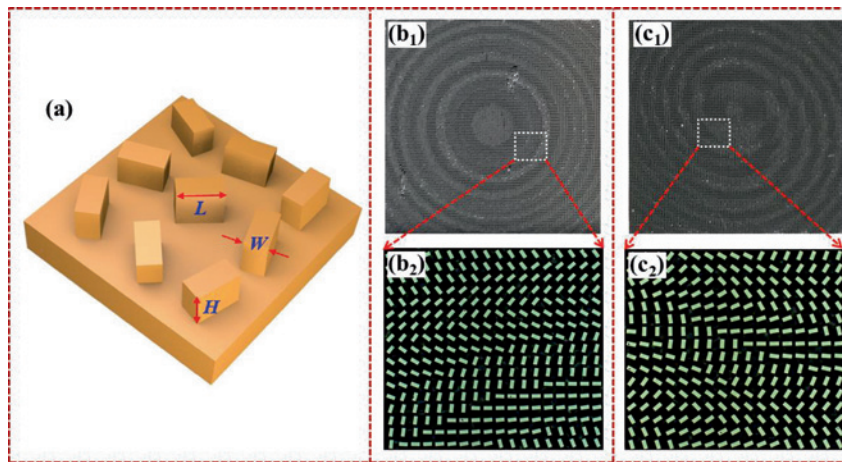
Figure 2: Schematic and fabrication of the spin Hall metalens. (a) Schematic of the spin Hall metalens consists of silicon micropillars with identical shape and different in-plane orientations deposited on a silicon substrate. (b_1) and (c_1) Optical image of the fabricated spin Hall metalenses that can manipulate photonics spin-dependent splitting in longitudinal direction and multiple dimensions, respectively. (b_2) and (c_2) Zoom-in images of part from (b_1) and (c_1), respectively.

LCP incident THz waves, we observe one focal point in the left side, while another one in the right side under the illumination of RCP THz waves (see Figure 3(c_1)), indicating a metalens with longitudinal spin-dependent splitting. The electric field distributions in the x-y plane also demonstrate that only one circular-shaped spot is observed at $z = 3.8$ mm (or $z = 6.6$ mm) for the incidence of LCP (or RCP) THz waves. Here, the intensities of these two helicity-dependent focal spots are different, which can be attributed to the different focal lengths. The experimental measurements of such spin Hall metalens are shown in Figure 3(d_1)~3(f_3). In experiment, the incident x-polarized LP THz beam is focused into two separated focal spots away from the sample, as shown in Figure 3(d_1). In comparison with Figure 3(a_1) and 3(d_1), both the numerical simulations and measured results are matched well with each other, except for a slight discrepancy in the size of focal spots. It can be attributed to the fabrication error and the non-perfect signal-to-noise ratio (SNR) of the THz source (in experiment). The electric field distributions for LCP and RCP incidence of THz waves are shown in Figure 3(e_1) and 3(f_1). The corresponding electric field distributions in the x-y plane are experimentally measured and shown in Figure 3(d_2)~3(f_2). The calculated focusing efficiencies for LCP and RCP incidences are 39 and 29.2%, respectively, while they are 26.1 and 16.2% in experiment. Here, the difference in efficiency may be attributed to the different numerical aperture of the spin-dependent focal points and the finite silicon pillars in metalens. In addition, the calculated and measured electric field distributions in the y-z plane and the corresponding Stokes parameters S_3 are given in Supplementary Materials Section 2. To further demonstrate the robust approach for manipulating spin photons, we also design a spin Hall metalens with structure parameters as follows: $x_i = x_j = y_i = y_j = 0$, $f_i = 3$ mm and

$f_j = 7$ mm. The numerical simulations, measurements and the corresponding Stokes parameters S_3 are also supplied in Supplementary Materials Section 3.

Now, we demonstrate a unique and robust approach (based on pure geometric phase) to realize the manipulation of photonic spin-dependent splitting in both longitudinal and transverse directions, as shown in Figure 4. The pre-designed structure parameters for this spin Hall metalens are $x_i = x_j = 0$, $y_i = 1.5$ mm, $y_j = -0.5$ mm, $f_i = 4$ mm and $f_j = 6$ mm. The numerical demonstration of multidimensional spin-dependent splitting under the illumination of an LP THz beam at 0.69 THz is illustrated in Figure 4(a_1). The two focal spots with longitudinal and transverse spin-dependent splitting are observed, and located with longitudinal centers at $z = 3.8$ mm and $z = 5.7$ mm, which are close to the designed values. The transverse (in y-direction) spin-dependent shift of these two focal spots is $\Delta y_1 \approx 1.5$ mm and $\Delta y_2 \approx -0.5$ mm, respectively. The corresponding electric field ($|E|^2$) distributions in the x-y plane are shown in Figure 4(a_2) and 4(a_3), respectively. Under the illumination of helicity-dependent THz waves, there is only one focal point located at either left side of the upper half space (see Figure 4(b_1)) or right side of the lower half space (see Figure 4(c_1)), demonstrating the manipulation of spin-dependent splitting in both longitudinal and transverse directions. The corresponding electric field ($|E|^2$) distributions in the x-y plane are simultaneously demonstrated the multidimensional manipulation of PSHE, as shown in Figure 4(b_2)~4(c_3). Figure 4(d_1)~4(f_1) show the measured results, in which there are two spin-dependent focal spots located at $z = 3.8$ mm and $z = 5.7$ mm, respectively. The x-y plane of electric field distributions are given in Figure 4(d_2)~4(f_3). Both the measured results and the numerical simulation are agreed well with each other. In this situation, the focusing efficiencies are 38.5 and 33.1% under the illumination of LCP and RCP THz
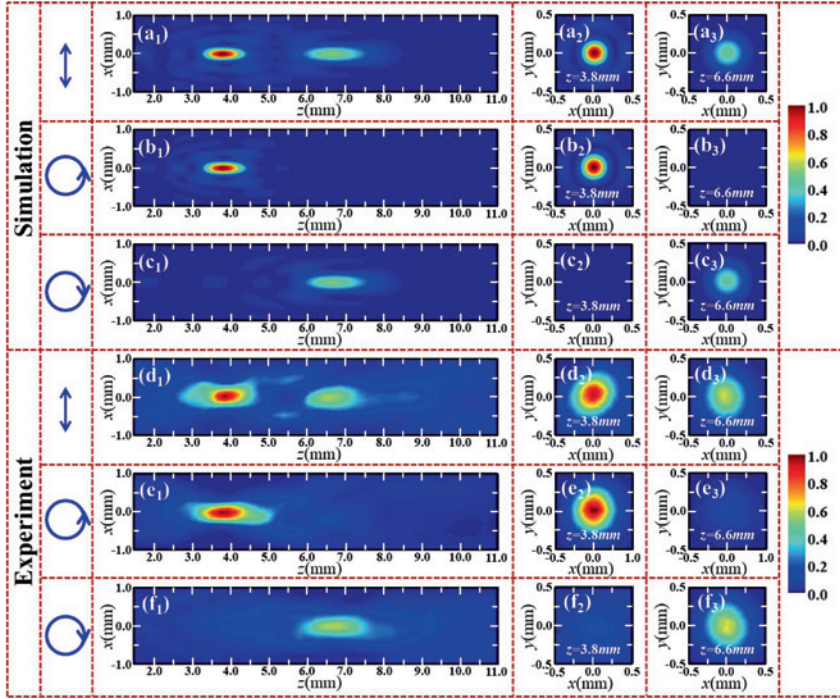
Figure 3: Electric field distributions ($|E|^2$) of the spin Hall metalens that can manipulate photonics spin-dependent splitting in the longitudinal direction. (a_1~c_1) Simulated electric field distributions for the transmitted THz waves in the *x-z* plane under the illumination of LP, LCP and RCP THz waves. (a_2~c_3) The corresponding electric field distributions in the *x-y* plane under the illumination of LP, LCP and RCP THz waves. (d_1~f_3) Corresponding experimental results.

waves, while they are 26.7 and 22.1% in measurement. The calculated Stokes parameters S_3 is supplied in Supplementary Materials Section 4. In addition, we have designed another spin Hall metalens that can manipulate photonic spin in multiple dimensions with structure parameters as: $x_i = x_j = 0$, $y_i = 1.5$ mm, $y_j = -0.5$ mm, $f_i = 4$ mm and $f_j = 7$ mm (see Supplementary Materials Section 5). In addition, our approach can be extended to manipulate spin-dependent splitting in three spatial dimensions (see the numerical simulations in Supplementary Materials Section 6).

To further demonstrate the characters of the spin-dependent splitting, a helicity-dependent sample is designed and fabricated, as shown in Figure 5(a) and (b). As a proof-of-concept, the helicity-dependent imaging is realized, when the helicity-dependent sample is embedded in two spin-dependent focal spots. Here, the designed sample consists of T-shaped meta-atoms and slit grating that are coated on each side of a polyimide (PI) film. Two helicity-dependent capital Letters "T" and "U" are composed of T-shaped meta-atoms with counterclockwise
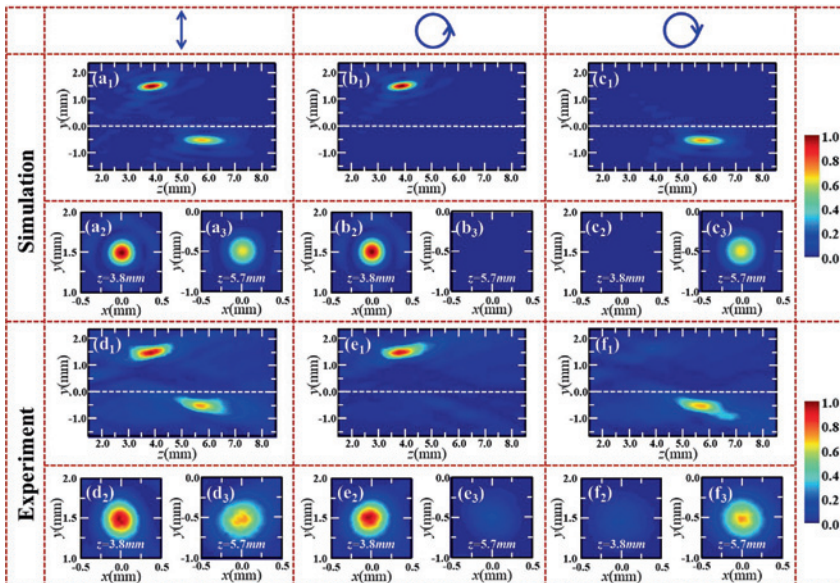

Figure 4: Electric field distributions ($|E|^2$) of the spin Hall metalens that can manipulate photonics spin-dependent splitting in both transverse and longitudinal directions. (a_1~c_1) Simulated electric field distributions for the transmitted THz waves in the *x-z* plane under the illumination of LP, LCP and RCP THz waves. (a_2~c_3) The corresponding electric field distributions in the *x-y* plane under the illumination of LP, LCP and RCP THz waves. (d_1~f_3) Corresponding experimental results.
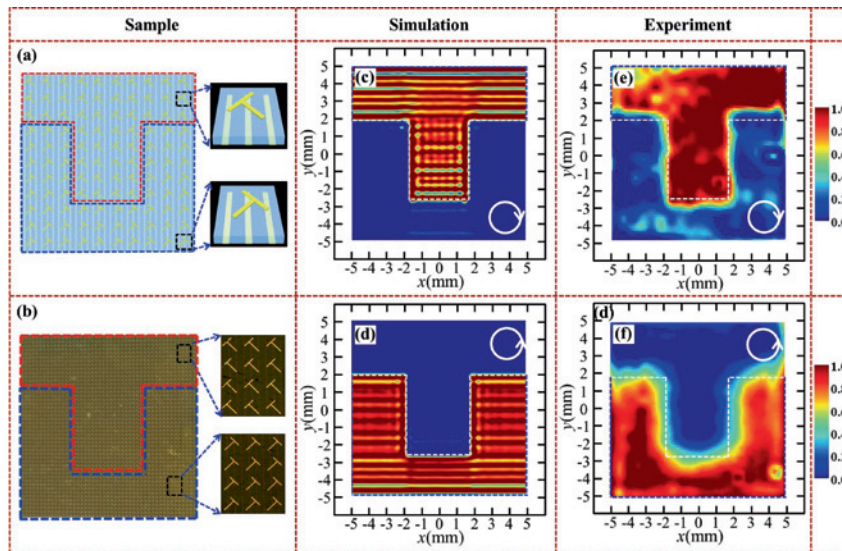
Figure 5: Helicity-dependent imaging. (a) and (b) Schematic and optical image of the imaging sample. (c) and (d) The simulated electric field distributions ($|E|^2$) of the helicity-dependent sample under the illumination of RCP and LCP THz waves. (c) and (d) The measured results when the helicity-dependent sample is embedded in the left and right focal points, respectively.

rotation of 45° and clockwise rotation of 45°, respectively. The numerical simulations of the transmission properties and working principle for the helicity-dependent imaging sample are given in Supplementary Materials Section 7. For simplicity, we use the metalens with longitudinal spin-splitting to demonstrate the helicity-dependent imaging, as shown in Figure 5(c)~5(f). Figure 5(c) illustrates the calculated electric field distribution under the illumination of RCP THz waves, and the capital Letter of "T" is revealed. Since the capital letter of "T" consists of T-shaped meta-atom arrays (coated on one side of the PI film) with counterclockwise rotation of 45° and slit gratings (coating on the other side of PI film), the RCP THz waves can be transmitted through the sample while the LCP THz waves is reflected, leading to the observation of the capital letter of "T". In contrast, the capital letter of "U" can be revealed under the illumination of LCP THz waves, as shown in Figure 5(d). In experiment, the capital Letter of "T" is observed when the sample is embedded in the left focal point (see Figure 5(e) for scanning imaging), while the capital letter of "U" is revealed when the sample is embedded in the right focal point (see Figure 5(f) for scanning imaging), demonstrating the helicity-dependent imaging. The helicity-dependent imaging based on multidimensional spin Hall metalens and the experimental scheme are given in Supplementary Materials Section 8 and 9.

4 Conclusion

In summary, we have proposed and experimentally demonstrated an approach to design multidimensional spin Hall metalens that can flexibly manipulate the spin-dependent splitting in both transverse and longitudinal directions using a single-layer dielectric metasurface. Position-controllable and spin-dependent focal points are realized based on the pure geometric phase. The flexible approach can be extended to manipulate spin-dependent splitting in three spatial dimensions. The helicity-dependent imaging capabilities are demonstrated by the spin Hall metalens and helicity-dependent sample. The simplicity and robust approach in manipulating SHE may provide a platform for designing future compact devices.

References

[1] M. Onoda, S. Murakami, and N. Nagaosa, "Hall effect of light," *Phys. Rev. Lett.*, vol. 93, no. 8, Art no. 083901, 2004.

[2] K. Y. Bliokh and Y. P. Bliokh, "Conservation of angular momentum, transverse shift, and spin Hall effect in reflection and refraction of an electromagnetic wave packet," *Phys. Rev. Lett.*, vol. 96, no. 7, Art no. 073903, 2006.

[3] O. Hosten, and P. Kwiat, "Observation of the spin Hall effect of light via weak measurements," *Science*, vol. 319, no. 5864, pp. 787–790, 2008.

[4] K. Y. Bliokh, Y. Gorodetski, V. Kleiner, et al., "Coriolis effect in optics: unified geometric phase and spin-Hall effect," *Phys. Rev. Lett.*, vol. 101, no. 3, Art no. 030404, 2008.

[5] Y. Qin, Y. Li, H. He, et al., "Measurement of spin Hall effect of reflected light," *Opt. Lett.*, vol. 34, no. 17, pp. 2551–2553, 2009.

[6] N. Shitrit, I. Bretner, Y. Gorodetski, et al., "Optical spin Hall effects in plasmonic chains," *Nano Lett.*, vol. 11, no. 5, pp. 2038–2042, 2011.

[7] K. Y. Bliokh, A. Niv, V. Kleiner, et al., "Geometrodynamics of spinning light," *Nat. Photonics*, vol. 2, no. 12, pp. 748–753, 2008.

[8] Y. Gorodetski, K. Y. Bliokh, B. Stein, et al., "Weak measurements of light chirality with a plasmonic slit," *Phys. Rev. Lett.*, vol. 109, no. 1, Art no. 013901, 2012.

[9] C. Prajapati, D. Ranganathan, and J. Joseph, "Spin Hall effect of light measured by interferometry," *Opt. Lett.*, vol. 38, no. 14, pp. 2459-2462, 2013.

[10] S. Chen, X. Ling, W. Shu, et al., "Precision measurement of the optical conductivity of atomically thin crystals via the photonic spin Hall effect," *Phys. Rev. Appl.*, vol. 13, no. 1, Art no. 014057, 2020.

[11] A. Silva, F. Monticone, G. Castaldi, et al., "Performing mathematical operations with metamaterials," *Science*, vol. 343, no. 6167, pp. 160–163, 2014.

[12] T. Zhu, Y. Zhou, Y. Lou, et al., "Plasmonic computing of spatial differentiation," *Nat. Commun.*, vol. 8, no. 1, p. 15391, 2017.

[13] T. Zhu, Y. Lou, Y. Zhou, et al., "Generalized spatial differentiation from the spin Hall effect of light and its application in image processing of edge detection," *Phys. Rev. Appl.*, vol. 11, no. 3, Art no. 034043, 2019.

[14] S. He, J. Zhou, S. Chen. et al., "Spatial differential operation and edge detection based on the geometric spin Hall effect of light," *Opt. Lett.*, vol. 45, no. 4, pp. 877–880, 2020.

[15] N. Yu, P. Genevet, M. A. Kats, et al., "Light propagation with phase discontinuities: generalized laws of reflection and refraction," *Science*, vol. 334, no. 6054, pp. 333–337, 2011.

[16] L. Huang, X. Chen, H. Mühlenbernd, et al., "Dispersionless phase discontinuities for controlling light propagation," *Nano Lett.*, vol. 12, no. 11, pp. 5750–5755, 2012.

[17] X. Chen, L. Huang, H. Mühlenbernd, et al., "Dual-polarity plasmonic metalens for visible light," *Nat. Commun.*, vol. 3, no. 1, p. 1198, 2012.

[18] X. Chen, M. Chen, M. Q. Mehmood, et al., "Longitudinal multifoci metalens for circularly polarized light," *Adv. Opt. Mater.*, vol. 3, no. 9, pp. 1201–1206, 2015.

[19] A. Arbabi, Y. Horie, M. Bagheri, et al., "Dielectric metasurfaces for complete control of phase and polarization with subwavelength spatial resolution and high transmission," *Nature Natecnnol.*, vol. 10, no. 11, pp. 937–943, 2015.

[20] M. Khorasaninejad, W. T. Chen, R. C. Devlin, et al., "Metalenses at visible wavelengths: Diffraction-limited focusing and subwavelength resolution imaging," *Science*, vol. 352, no. 6290, pp. 1190–1194, 2016.

[21] W. T. Chen, A. Y. Zhu, V. Sanjeev, et al., "A broadband achromatic metalens for focusing and imaging in the visible," *Nat. Nanotechnol.*, vol. 13, no. 3, pp. 220–226, 2018.

[22] S. Wang, P. C. Wu, V. C. Su, et al., "A broadband achromatic metalens in the visible," *Nat. Nanotechnol.*, vol. 13, no. 3, pp. 227–232, 2018.

[23] R. J. Lin, V. C. Su, S. Wang, et al., "Achromatic metalens array for full-colour light-field imaging," *Nat. Nanotechnol.*, vol. 14, no. 3, pp. 227–231, 2019.

[24] X. Ni, Z. J. Wong, M. Mrejen, et al., "An ultrathin invisibility skin cloak for visible light," *Science*, vol. 349, no. 6254, pp. 1310–1314, 2015.

[25] X. Ni, A. V. Kildishev, and V. M. Shalaev, "Metasurface holograms for visible light," *Nat. Commun.*, vol. 4, no. 1, p. 2807, 2013.

[26] G. Zheng, H. Mühlenbernd, M. Kenney, et al., "Metasurface holograms reaching 80% efficiency," *Nat. Nanotechnol.*, vol. 10, no. 4, pp. 308–312, 2015.

[27] D. Wen, F. Yue, G. Li, et al., "Helicity multiplexed broadband metasurface holograms," *Nat. Commun.*, vol. 6, no. 1, p. 8241, 2015.

[28] Y. W. Huang, W. T. Chen, W. Y. Tsai, et al., "Aluminum plasmonic multicolor meta-hologram," *Nano Lett.*, vol. 15, no. 5, pp. 3122–3127, 2015.

[29] X. Li, L. Chen, Y. Li, et al., "Multicolor 3D meta-holography by broadband plasmonic modulation," *Sci. Adv.*, vol. 2, no. 11, pp. e1601102, 2016.

[30] Z. Yue, G. Xue, J. Liu, et al., "Nanometric holograms based on a topological insulator material," *Nat. Commun.*, vol. 8, no. 1, pp. 15354, 2017.

[31] L. Jin, Z. Dong, S. Mei, et al., "Noninterleaved metasurface for (26-1) spin-and wavelength-encoded holograms," *Nano Lett.*, vol. 18, no. 12, pp. 8016–8024, 2018.

[32] L. Jin, Y. W. Huang, Z. Jin, et al., "Dielectric multi-momentum meta-transformer in the visible," *Nat. Commun.*, vol. 10, no. 1, pp. 4789, 2019.

[33] N. Yu, F. Aieta, P. Genevet, et al., "A broadband, background-free quarter-wave plate based on plasmonic metasurfaces," *Nano Lett.*, vol. 12, no. 12, pp. 6328–6333, 2012.

[34] N. K. Grady, J. E. Heyes, D. R. Chowdhury, et al., "Terahertz metamaterials for linear polarization conversion and anomalous refraction," *Science*, vol. 340, no. 6138, pp. 1304–1307, 2013.

[35] R. H. Fan, Y. Zhou, X. P. Ren, et al., "Freely tunable broadband polarization rotator for terahertz waves," *Adv. Mater.*, vol. 27, no. 7, pp. 1201–1206, 2015.

[36] P. Yu, J. Li, C. Tang, et al., "Controllable optical activity with non-chiral plasmonic metasurfaces," *Light Sci. Appl.*, vol. 5, no. 7, p. e16096, 2016.

[37] M. Pu, X. Li, X. Ma, et al., "Catenary optics for achromatic generation of perfect optical angular momentum," *Sci. Adv.*, vol. 1, no. 9, p. e1500396, 2015.

[38] M. Q. Mehmood, S. Mei, S. Hussain, et al., "Visible-frequency metasurface for structuring and spatially multiplexing optical vortices," *Adv. Mater.*, vol. 28, no. 13, pp. 2533–2539, 2016.

[39] F. Yue, D. Wen, C. Zhang, et al., "Multichannel polarization-controllable superpositions of orbital angular momentum states," *Adv. Mater.*, vol. 29, no. 15, p. 1603838, 2017.

[40] X. F. Zang, Y. M. Zhu, C. X. Mao, et al., "Manipulating terahertz plasmonic vortex based on geometric and dynamic phase," *Adv. Opt. Mater.*, vol. 7, no. 3, p. 1801328, 2019.

[41] G. Li, S. Chen, N. Pholchai, et al., "Continuous control of the nonlinearity phase for harmonic generations," *Nat. Mater.*, vol. 14, no. 6, pp. 607–612, 2015.

[42] W. Ye, F. Zeuner, X. Li, et al., "Spin and wavelength multiplexed nonlinear metasurface holography," *Nat. Commun.*, vol. 7, no. 1, p. 11930, 2016.

[43] F. Walter, G. Li, C. Meier, et al., "Ultrathin nonlinear metasurface for optical image encoding," *Nano Lett.*, vol. 17, no. 5, pp. 3171–3175, 2017.

[44] Z. Li, W. Liu, Z. Li, et al., "Tripling the capacity of optical vortices by nonlinear metasurface," *Laser Photon. Rev.*, vol. 12, no. 11, p. 1800164, 2018.

[45] G. Hu, X. Hong, K. Wang, et al., "Coherent steering of nonlinear chiral valley photons with a synthetic Au–WS 2 metasurface," *Nat. Photon.*, vol. 13, no. 7, pp. 467–472, 2019.

[46] J. Zhou, H. Qian, C. Chen, et al., "Optical edge detection based on high-efficiency dielectric metasurface," *Proc. Natl. Acad. Sci. USA*, vol. 116, no. 23, pp. 11137–11140, 2019.

[47] H. Kwon, D. Sounas, A. Cordaro, et al., "Nonlocal metasurfaces for optical signal processing," *Phys. Rev. Lett.*, vol. 121, no. 17, p. 173004, 2018.

[48] A. Momeni, H. Rajabalipanah, A. Abdolali, et al., "Generalized optical signal processing based on multioperator metasurfaces synthesized by susceptibility tensors," *Phys. Rev. Appl.*, vol. 11, no. 6, Art no. 064042, 2019.

[49] Y. Zhou, H. Zheng, I. Kravchenko, et al., "Flat optics for image differentiation," *Nat. Photon.*, 2020, https://doi.org/10.1038/s41566-020-0591-3.

[50] J. Lin, J. P. B. Mueller, Q. Wang, et al., "Polarization-controlled tunable directional coupling of surface plasmon polaritons," *Science*, vol. 340, no. 6130, pp. 331–334, 2013.

[51] Q. Xu, X. Zhang, Y. Xu, et al., "Polarization-controlled surface plasmon holography," *Laser Photon. Rev.*, vol. 11, no. 1, pp. 1600212, 2017.

[52] G. Spektor, A. David, B. Gjonaj, et al., "Metafocusing by a metaspiral plasmonic lens," *Nano. Lett.*, vol. 15, no. 9, pp. 5739–5743, 2015.

[53] X. Yin, Z. Ye, J. Rho, et al., "Photonic spin Hall effect at metasurfaces," *Science*, vol. 339, no. 1405–1407, pp. 6126, 2013.

[54] X. Ling, X. Zhou, X. Yi, et al., "Giant photonic spin Hall effect in momentum space in a structured metamaterial with spatially varying birefringence," *Light Sci. Appl.*, vol. 4, no. 5, p. e290, 2015.

[55] W. Luo, S. Xiao, Q. He, et al., "Photonic spin Hall effect with nearly 100% efficiency," *Adv. Opt. Mater.*, vol. 3, no. 8, pp. 1102–1108, 2015.

[56] X. G. Luo, M. B. Pu, X. Li, et al., "Broadband spin Hall effect of light in single nanoapertures," *Light Sci. Appl.*, vol. 6, no. 9, p. e16276, 2017.

[57] X. Ling, X. Zhou, K. Huang, et al., "Recent advances in the spin Hall effect of light," *Rep. Prog. Phys.*, vol. 80, no. 6, p. 66401, 2017.

[58] H. X. Xu, G. Hu, Y. Li, et al., "Interference-assisted kaleidoscopic meta-plexer for arbitrary spin-wavefront manipulation," *Light Sci. Appl.*, vol. 8, no. 1, p. 3, 2019.

[59] J. Zhou, H. Qian, G. Hu, et al., "Broadband photonic spin Hall meta-lens," *ACS Nano.*, vol. 12, no. 1, pp. 82–88, 2018.

[60] S. Li, X. Li, G. Wang, et al., "Multidimensional manipulation of photonic spin Hall effect with a single-layer dielectric metasurface," *Adv. Opt. Mater.*, vol. 7, no. 5, p. 1801365, 2019.

[61] X. F. Zang, W. W. Xu, M. Gu, et al., "Polarization-insensitive metalens with extended focal depth and longitudinal high-tolerance imaging," *Adv. Opt. Mater.*, vol. 8, no. 2, p. 1901342, 2020.

[62] X. F. Zang, C. X. Mao, X. G. Guo, et al., "Polarization-controlled terahertz super-focusing," *Appl. Phys. Lett.*, vol. 113, no. 7, p. 071102, 2018.

[63] L. Chen, Y. M. Wei, X. F. Zang, et al., "Excitation of dark multipolar plasmonic resonances at terahertz frequencies," *Sci. Rep.*, vol. 6, no. 1, p. 22027, 2016.

[64] L. Chen, D. Liao, X. Guo, et al., "Terahertz time-domain spectroscopy and micro-cavity components for probing samples: a review," *Front. Inform. Tech. Electronic Eng.*, vol. 20, no. 5, pp. 591–607, 2019.